Alternatives and Limitations of Off-the-Shelf Power Management Circuits for Low-Power Thermoelectric Generators

Filippo Leoncini , Mohamad Ridwan , Ferran Reverter *

Posted Date: 21 May 2026

doi: 10.20944/preprints202605.1451.v1

Keywords: energy harvesting; maximum power point tracker (MPPT); power management circuit (PMC); thermoelectric generator (TEG)

 doi:10.20944/preprints202605.1451.v1

Article

Alternatives and Limitations of Off-the-Shelf Power Management Circuits for Low-Power Thermoelectric Generators

Filippo Leoncini [1], Mohamad Ridwan [2] and Ferran Reverter [2,*]

[1] Department of Information Engineering, Università Degli Studi di Brescia, Brescia, Italy
[2] Department of Electronic Engineering, Universitat Politècnica de Catalunya—BarcelonaTech, 08860 Castelldefels, Spain
* Correspondence: ferran.reverter@upc.edu; Tel.: +34 934137076

Abstract

In the field of power management circuits (PMC) for low-power thermoelectric generators (TEG) intended for autonomous sensors, this article experimentally evaluates the alternatives commercially available. Considering their limitations in terms of minimum input voltage and power efficiency, this article also proposes and experimentally characterizes a circuit topology that combines and interconnects two different PMC alternatives so as to achieve the benefits of b oth. Thanks to this interconnection, the resulting circuit is able to start operating from a low input voltage (i.e., 40 mV of TEG open-circuit voltage), which is really attractive for TEGs under low thermal gradients, with a satisfactory power efficiency (i.e., up to 78 %).

Keywords: energy harvesting; maximum power point tracker (MPPT); power management circuit (PMC); thermoelectric generator (TEG)

1. Introduction

The twin green and digital transition of our society promotes the application of digital technologies in a sustainable approach. The Internet of Things (IoT) is an example of digital technology that involves the interconnection of many sensor nodes with the aim of gathering information about the status of a system/process, such as a smart building, industrial process, or railway system [1]. It is projected that half of these IoT sensors will be located indoors [2], which is the scenario of interest herein. A large-scale deployment of these IoT sensors is no exempt from limitations, and probably the most critical issue is their power supply [3]. Wired-power solutions are impractical in inaccessible locations or in scenarios involving a large number of sensors. Batteries have a finite lifespan, involve maintenance costs, and pose environmental concerns due to disposal and recycling issues. Accordingly, the most viable and sustainable alternative to power IoT sensors seems to be the use of an energy harvester, which converts "free" environment energy to electrical energy.

Energy harvesters can rely on different types of input energy [4]: optical [5,6], thermal [7,8], mechanical [9,10], and radio frequency [11]. This article focuses on thermal energy harvesters based on a thermoelectric generator (TEG), which is a solid-state device made of multiple p-type and n-type semiconductor junctions, that converts a thermal gradient into electrical energy [12,13]. TEG-based systems offer several advantages, for example, in comparison to mechanical energy harvesters, they operate silently without any moving part. However, in indoor domestic scenarios, TEGs undergo two significant constraints: 1) the available thermal gradients are generally reduced, and 2) the physical space for installing the TEG (and the corresponding heatsink for the heat transfer) is often limited by the geometry of the thermal energy source itself and/or the surrounding installation area. As a consequence of that, the output power for a low-area TEG (say, a few tens of cm^2) is usually in the range of units or tens of milliwatt, but it can drop to the microwatt range in wearable applications [8].

 doi:10.20944/preprints202605.1451.v1

The electrical output of a TEG is generally modeled by a Thévenin equivalent circuit, with a voltage source (equal to the open-circuit voltage, V_{OC}) in series with an internal resistance (R_{TEG}). This voltage is a DC magnitude, yet generally this is not valid to directly power the electronics of the sensor node. For this reason, an intermediate power management circuit (PMC) is required to adapt the DC voltage level at the TEG output to the DC voltage level needed by the sensor electronics. This DC/DC conversion has to be performed with a high efficiency so as to maximize the power extraction. This means, among others, that the TEG should operate around its maximum power point (MPP), which corresponds to an operating voltage equal to half of V_{OC} [14]. This can be obtained, for example, by applying the fractional open-circuit voltage (FOCV) [15] as an MPP tracking (MPPT) technique with a ratio of 0.5, although other techniques such as the perturb and observe have also been suggested [16]. On the semiconductor market, two different types of PMC designed for TEGs can be found. On the one hand, there are PMCs able to operate from a very low input voltage, which is really necessary for TEGs under low thermal gradients, but without the ability to apply any MPPT method. On the other hand, PMCs able to apply an MPPT method but operating from higher values of input voltage. To the best of our knowledge, off-the-shelf PMCs for TEGs offering both abilities (i.e., low input voltage operation and MPPT) are not available, although these have been suggested with application specific integrated circuits [14,17].

In the previous context, the first goal of this article is to evaluate the advantages and limitations of the two main PMC alternatives commercially available to handle the power coming from low-area TEG located indoors. Afterwards, the second goal is the proposal and experimental characterization of a circuit that combines the two conventional PMC alternatives so as to achieve the benefits of both, i.e., low input voltage operation and MPPT functionality.

The rest of this article is organized as follows. Section 2 provides information about the TEG that is used as a reference for the ensuing characterization of the PMCs. Section 3 explains general issues related to the instrumentation and efficiency estimation. Sections 4 and 5 explain the operating principle and discuss the experimental results of the two conventional off-the-shelf PMC alternatives working independently. Section 6 proposes the interconnection of the two PMC alternatives and provides the corresponding experimental results. Finally, Section 7 concludes this article.

2. TEG

For the evaluation of the PMCs carried out in the next sections, a commercial TEG was considered as a reference for the input signal. This is the GM250-241-10-12 from European Thermodynamics with an active area of 40×40 mm^2. This TEG was experimentally characterized as follows. The hot side of the TEG was coupled to a thermal plate (QInstruments ColdPlate 2016-0110), whereas the cold side was attached to a heatsink (TDEX6015/TH with a dimension of 60×60×47 mm^2) so as to dissipate the heat to the ambient. With this topology, the TEG was subjected to thermal gradients (ΔT) from 5 to 40ºC, which are expected in indoor applications [18]; this ΔT corresponds to the difference between the temperature of the thermal plate and the ambient temperature. The TEG output was connected to a source and measurement unit (Keithley 2450) to extract its current-voltage characteristic for the different conditions under test.

The experimental results of the preliminary test of this TEG are shown in Figures 1 and 2. From Figure 1, in the range of ΔT under test, V_{OC} ranged from 38 to 483 mV, whereas the power at MPP ranged from 60 μW to 7 mW. Note that the TEG output voltage is really low at low levels of ΔT, clearly lower than the minimum operating voltage of the second group of PMC indicated in Section 1. On the other hand, Figure 2 shows the dependence of R_{TEG} on ΔT; this resistance was calculated as the open-circuit voltage divided by the short-circuit current. Accordingly, R_{TEG} was between 6 and 9 Ω. The higher the value of ΔT, the higher R_{TEG}. The previous values of V_{OC} and R_{TEG} will be used in the following sections for the characterization of the PMCs.

 doi:10.20944/preprints202605.1451.v1

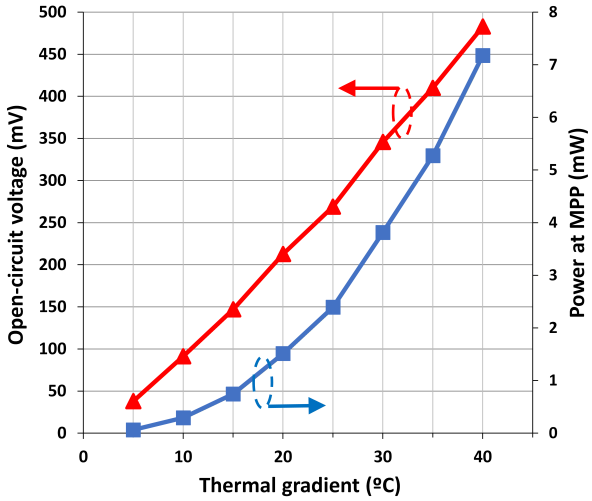

Figure 1. Open-circuit voltage and power at MPP versus thermal gradient for the TEG under test.

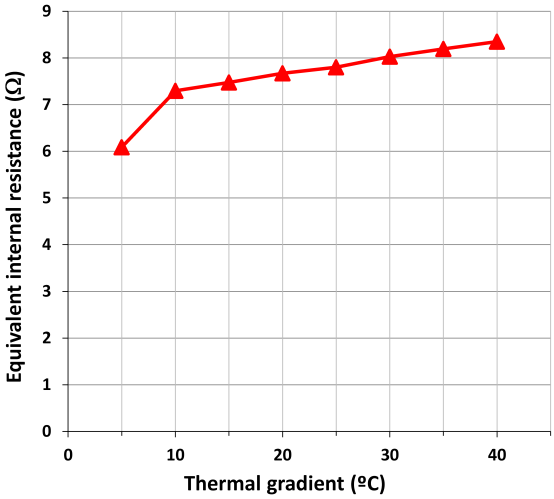

Figure 2. Equivalent internal resistance versus thermal gradient for the TEG under test.

3. Instrumentation and Efficiency

In order to characterize the PMCs independently of potential drifts affecting the TEG, this was emulated by a source and measurement unit (SMU-1, Keysight B2961A) with a resistor connected in series. The considered values of V_{OC} and R_{TEG} were in agreement with those obtained in Section 2. On the other hand, the PMC output was connected to another source and measurement unit (SMU-2, Agilent B2901A) behaving as a voltage source (3 V) to emulate an energy storage element (such as a supercapacitor or a rechargeable battery) that powers the sensor electronics when the thermal energy is not sufficient. The voltage and current at the input were measured by SMU-1, whereas the same was carried out at the output by SMU-2. All measurements were repeated 50 times, and then those were averaged. In addition, both SMUs were configured with a measuring (integration) time of 200 ms [i.e., Number of Period Line Cycles (NPLC) = 10] to reduce the noise effects on the measurement. BenchVue software (Keysight) was employed to automatically control the sequence of operations and measurements. The components employed in the different setups are summarized in Table 1.

 doi:10.20944/preprints202605.1451.v1

Table 1. Value of the components employed in the experiments to test the PMCs.

Component	Value	Component	Value
R_1	4.7 MΩ [a]	L_1	7.5 μH
R_2	4.7 MΩ [a]	L_2	75 mH
R_3	170 MΩ [b]	C_1	1 nF
R_4	10 MΩ [b]	C_2	330 pF
C_{in}	330 μF	C_{out}	220 μF

[a] Selected to have a FOCV ratio of 0.5. [b] Selected to have V_{ref} = 200 mV at 3.6 V of supply voltage.

Regarding the estimation of the power efficiency of the PMC, two contributions need to be considered [15]: 1) the efficiency of the tracking (η_{track}), and 2) the efficiency of the circuit ($\eta_{DC/DC}$) that carries out the DC/DC conversion. The first one depends on the ability of the circuit to follow the MPP of the TEG, and can be expressed as:

$$\eta_{track} = \frac{P_{AOP}}{P_{MPP}}, \tag{1}$$

where P_{MPP} is the power provided by the TEG when this operates at the MPP, whereas P_{AOP} is the power provided by the TEG at the actual operating point (AOP). Applying the maximum power transfer theorem, P_{MPP} can be found as:

$$P_{MPP} = \frac{V_{OC}^2}{4R_{TEG}}. \tag{2}$$

On the other hand, the second contribution of efficiency is equal to:

$$\eta_{DC/DC} = \frac{P_{out}}{P_{AOP}}, \tag{3}$$

which relates the power obtained at the output of the PMC (P_{out}) with the actual power that is applied to the input (i.e., P_{AOP}). Therefore, the overall efficiency (η_T) can be expressed as:

$$\eta_T = \eta_{track}\eta_{DC/DC} = \frac{P_{out}}{P_{MPP}} = \frac{4P_{out}R_{TEG}}{V_{OC}^2} \tag{4}$$

The efficiencies of the PMCs in Sections 4, 5, and 6 were experimentally evaluated and compared to each other using (4), where P_{out} was obtained from SMU-2, V_{OC} from SMU-1, and R_{TEG} was the resistance physically placed in the setup to emulate the internal resistance of the TEG. Note that in some references of the literature (e.g., [14,17]), the efficiency was calculated considering only the contribution in (3). This is a good estimation of the converter efficiency but it does not ensure a good impedance matching at the input and, hence, the information reported there is incomplete.

4. First PMC Alternative

As indicated in Section 1, the first alternative to manage the power coming from a TEG corresponds to a PMC able to operate from a very low input voltage, but without the ability to apply any MPPT method. Examples of commercial chips that belong to this category are: LTC3108 (Analog Devices) and EM8900 (EM Microelectronic).

4.1. Operating Principle

This type of PMC generally relies on a resonant step-up oscillator formed by an external step-up transformer, some external capacitors, and an internal MOSFET (connected at the SW pin in the case of the LTC3108), as shown in Figure 3. The AC voltage produced at the secondary winding of the transformer is then internally rectified so as to generate a DC voltage at the output. With the same idea

 doi:10.20944/preprints202605.1451.v1

but with the goal of having a more compact design, a transformer-free self-powered oscillator made of off-the-shelf components was suggested in [19]. Alternatively, the transformer was embedded into the chip in the custom design proposed in [20].

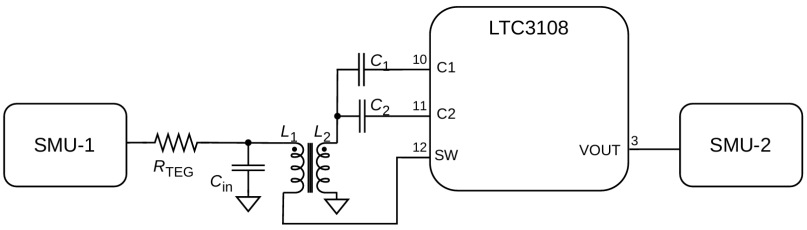

Figure 3. Setup and circuit to test the first PMC alternative to manage the power coming from a TEG.

EM8900 and LTC3108 are able to handle input voltages as low as 5 and 20 mV, respectively, which is very appropriate for TEGs under low gradients of temperature. However, according to their datasheet, the input resistance (and, hence, the ability to be adapted to the TEG internal resistance) depends on several factors. For example, in the LTC3108, the input resistance depends on both the applied input voltage and the ratio of the transformer. For a 1:100 ratio (which is the one employed herein), the input resistance decreases from 6 to 2.5 Ω with increasing the input voltage. Accordingly, the impedance matching and, hence, the tracking efficiency are expected to be low in this topology.

4.2. Experimental Results and Discussion

The circuit in Figure 3 was experimentally tested using the LTC3108; it was decided to test that chip instead of EM8900 since it is more often employed in the literature [21–23]. The experimental results of overall efficiency are represented in Figure 4 versus V_{OC} for different values of R_{TEG}. Several conclusions can be drawn from Figure 4: 1) the efficiency was low, with a maximum value of 28 % at $V_{OC} \approx 80$ mV and $R_{TEG} = 7$ Ω; 2) the efficiency tended to decrease with increasing V_{OC}, with a value lower than 12 % at $V_{OC} = 500$ mV; 3) for $V_{OC} < 200$ mV, the efficiency was slightly better for lower values of R_{TEG}; and 4) the minimum voltage for the operation of the LTC3108 was $V_{OC} = 40$ mV. Assuming an ideal impedance matching, this corresponds to an input voltage applied to the chip of 20 mV, which agrees with that provided into the datasheet.

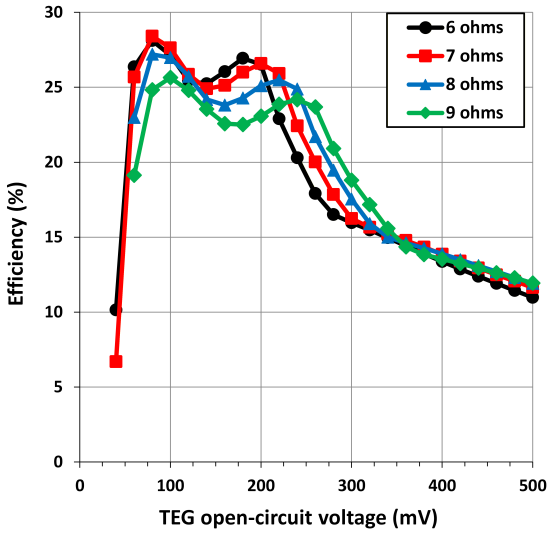

Figure 4. Experimental results of power efficiency from the circuit in Figure 3 for different values of R_{TEG}.

5. Second PMC Alternative

The second alternative corresponds to a PMC able to apply an MPPT method but operating from higher values of input voltage. Common commercial chips corresponding to this category are:

 doi:10.20944/preprints202605.1451.v1

ADP5092 (Analog Devices), BQ25570 (Texas Instruments), and AEM20940 (E-peas). For cold start, their minimum input voltage is 380, 600, and 380 mV, whereas, after cold start, it is 80, 100, and 50 mV, respectively.

5.1. Operating Principle

The first stage of these PMCs rely on an inductor-based boost DC/DC converter intended to regulate the operating voltage of the energy harvester [24]; the inductor is generally off-chip, but it is not represented in Figure 5. The previous three commercial PMCs can apply the FOCV technique. The FOCV ratio is set externally by means of a voltage divider implemented by high-value resistors (R_1 and R_2 in Figure 5) [15]. For a TEG, these two resistors need to be equal so that the FOCV ratio is 0.5. In such conditions, the input voltage of the PMC (VIN in Figure 5) is regulated around half of the open-circuit voltage and, hence, the equivalent input impedance of the PMC becomes equal to the internal resistance of the TEG.

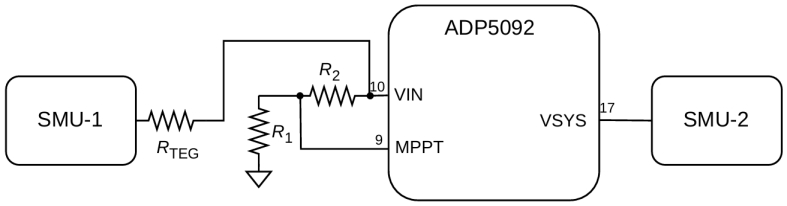

Figure 5. Setup and circuit to test the second PMC alternative to manage the power coming from a TEG.

5.2. Experimental Results and Discussion

The overall efficiency of the circuit in Figure 5 was experimentally evaluated using the ADP5092. The results are summarized in Figure 6 for different values of R_{TEG}; these were achieved by starting the test from the highest voltage (i.e., 500 mV) and then decreasing it, so as to be sure that ADP5092 was operating after the cold start. The following conclusions can be extracted from Figure 6: 1) the efficiency was remarkably high, with a maximum value of around 78 % at $V_{OC} = 500$ mV; 2) the efficiency tended to increase with increasing V_{OC}; 3) approximately in the range from 300 to 500 mV, the efficiency was moderately better for higher values of R_{TEG}; and 4) the minimum voltage for the operation of ADP5092 was $V_{OC} = 160$ mV at $R_{TEG} = 6\ \Omega$; this voltage was higher (to be precise, 200 mV) for the other values of R_{TEG} under test. Considering an ideal impedance matching at the input, this minimum voltage of 160 mV corresponds to an input voltage applied to the chip of 80 mV, which again agrees with that provided into the datasheet. Therefore, the minimum operating voltage of the circuit in Figure 5 is four times higher than that in Figure 3, whenever the cold-start phase has been surpassed.

 doi:10.20944/preprints202605.1451.v1

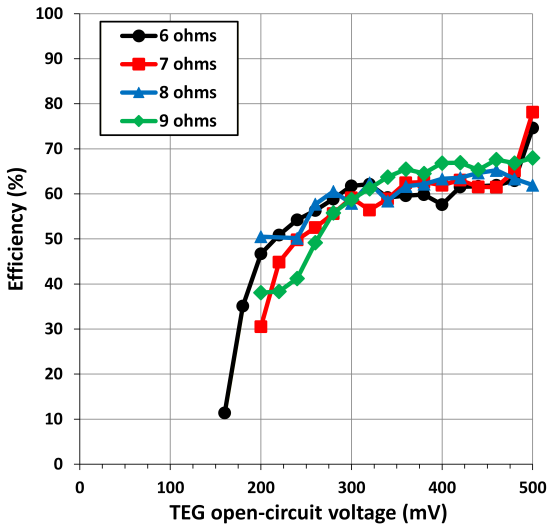

Figure 6. Experimental results of power efficiency from the circuit in Figure 5 for different values of R_{TEG}.

6. Both PMC Alternatives Interconnected

Assuming the low input voltage operation of the circuit in Figure 3 and the high efficiency of the circuit in Figure 5, it is suggested to combine them in a cascade topology to achieve the benefits of both. The idea of connecting these two types of PMC in cascade (to be precise, LTC3108 and BQ25504) was also suggested in [22], but with two significant limitations: 1) two switches were required between the output of the first stage and the input of the second stage, and 2) the comparator (which was in charge of controlling the switches) employed the signal connected to the transformer primary as an input, but this is neither a DC signal nor a reliable sample of the TEG output voltage due to the bad impedance matching with the LTC3108 input. On the other hand, LTC3108 and BQ25570 were proposed to be connected in parallel in [23]. However, for the characterization of the overall PMC, the internal resistance of the TEG was neglected and, hence, the efficiency results reported there are not representative of a real scenario.

6.1. Operating Principle

A block diagram of the proposed circuit is represented in Figure 7, whereas the complete schematic is depicted in Figure 8. In addition to the topologies shown before in Figures 3 and 5, the circuit in Figure 8 includes two switches (S1 and S2), a comparator (CMP), and a control unit. Another significant difference with respect to Figure 5 is the use of an auxiliary input (identified as BACKUP) in ADP5092. The two inputs (VIN and BACKUP) of ADP5092 are internally multiplexed toward the output (VSYS). The BACKUP input is selected when no signal is applied to VIN, and it is directly connected to VSYS. On the other hand, when a signal is applied to VIN, this is connected to VSYS through the boost DC/DC converter indicated in Section 5. In addition, an initial use of the BACKUP input enables to bypass the cold startup in ADP5092 and, hence, this can start operating from a lower input voltage applied to VIN input.

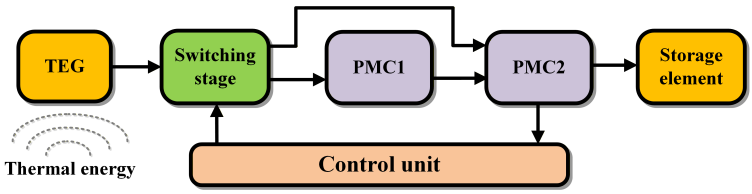

Figure 7. Block diagram of the proposed circuit combining the solutions in Sections 4 and 5.

Preprints.org (www.preprints.org) | NOT PEER-REVIEWED | Posted: 21 May 2026 doi:10.20944/preprints202605.1451.v1

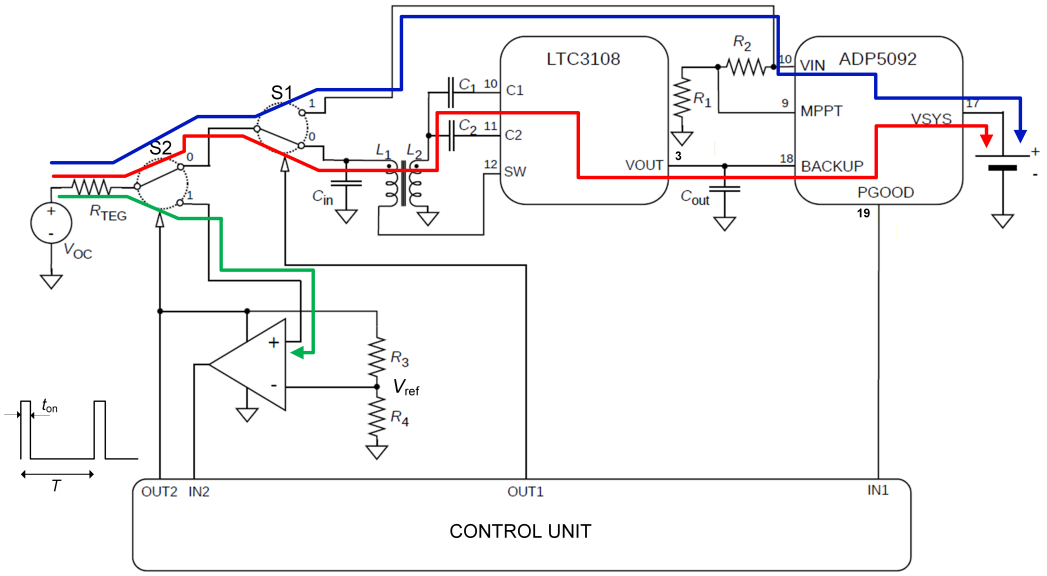

Figure 8. PMC combining the circuits in Figures 3 and 5 to manage the power coming from a TEG. The path in phases 1, 2, and 3 is indicated in red, blue, and green, respectively.

Table 2 summarizes the operation of the circuit in Figure 8 depending on the position of the switches. The circuit first operates in phase #1 (highlighted in red in Figure 8), so that the TEG is connected to LTC3108, and the LTC output is connected to the BACKUP input of ADP5092. In those conditions, the LTC output voltage linearly increases with time. When this voltage surpasses a certain level, an auxiliary output (identified as PGOOD) in ADP5092 is activated. When the control unit detects such an activation (via the digital input IN1), the digital output OUT2 becomes a pulse waveform with a period T and an on-time t_{on}; T is expected to be quite long (e.g., 1 minute), whereas t_{on} a few milliseconds. Therefore, every T, OUT2 is a high logic level during t_{on} and, hence, the circuit moves to phase #3 (highlighted in green in Figure 8). Then, V_{OC} is compared to a reference voltage V_{ref}, which corresponds to the minimum voltage that ensures the correct operation of ADP5092. According to Figure 6, this reference voltage was selected to be 200 mV, which was generated by a voltage divider implemented by R_3 and R_4. If $V_{OC} < V_{ref}$, the CMP output (and, hence, the digital input IN2) are in a low logic level, and the control unit decides to keep the circuit in phase #1. However, if $V_{OC} > V_{ref}$, the CMP output (and, hence, IN2) become a high logic level. This changes the digital output OUT1 to a high logic level so that the circuit moves to phase #2 (highlighted in blue in Figure 8), in which the TEG is directly connected to the VIN input of ADP5092.

Table 2. Operation phases of the circuit in Figure 8 depending on the position of the switches.

Phase	Position of S2	Position of S1	TEG connection
1	0	0	Connected to LTC
2	0	1	Connected to ADP
3	1	X	Connected to CMP [a]

[a] In open-circuit conditions.

6.2. Materials and Method

The circuit in Figure 8 was built using the same devices and components indicated in Sections 3-5. In addition, S1 and S2 were implemented by ADG839 (Analog Devices). This is a rail-to-rail solid-state switch with an ultra-low on-resistance (0.35 Ω typical). Note that this resistance has to be much smaller than R_{TEG} in order to ensure a good tracking of the MPP. Further, this switch offers an ultra low power consumption (3 nA typical). Assuming a supply voltage of 3 V, the resulting power consumption per switch is 9 nW, which is much lower (at least, a factor of 10^4) than the average power extracted from a

 doi:10.20944/preprints202605.1451.v1

low-area TEG in indoor applications [18]. In this experimental phase, the switches were powered by a DC power supply (Keysight E36441A). However, in a final prototype, these would be powered by the storage element of the sensor node.

The selected CMP was OPA379, which is a rail-to-rail operational amplifier with a typical current consumption is 2.9 μA. This could be optimized by selecting a nanopower comparator, such as TLV3691 with a current consumption is 75 nA. It is worth highlighting, however, that OUT2 in Figure 8 is also in charge of powering the CMP and the voltage divider (with $V_{\text{ref}} \approx$ 200 mV) and, hence, these sub-circuits only consume power during t_{on}.

As a proof of concept, the algorithm of the control unit was executed manually by providing the appropriate control signals to the switches using the same DC power supply indicated before. However, in a final prototype, the algorithm would be implemented by the microcontroller that, in most sensor nodes, is already available to carry out the sensing, processing, and transmitting tasks. Accordingly, neither extra cost nor extra power consumption is expected in this regard. A picture of the complete experimental setup to test the circuit in Figure 8 is shown in Figure 9, where SMU-1 and SMU-2 emulate, respectively, the TEG and the rechargeable battery, as already indicated in Section 3.

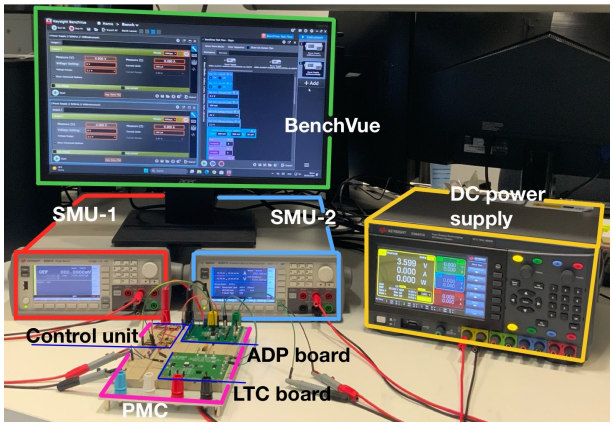

Figure 9. Experimental setup to test the circuit in Figure 8 under laboratory-controlled conditions.

6.3. Experimental Results and Discussion

The experimental results of power efficiency of the circuit in Figure 8 are represented in Figure 10, again for different values of R_{TEG}. Note that measurements were carried out after an initial transient required to charge the output capacitance of LTC3108 to a certain voltage; the length of this transient depended on the level of V_{OC}, but it was a few seconds for the conditions under test. According to Figure 10, for $V_{\text{OC}} < 200$ mV (i.e., when the TEG was connected to LTC3108), the efficiency of the overall circuit was almost identical to that obtained in Figure 4 in the same range. This is because, in such operating conditions, BACKUP input and VSYS output of the ADP5092 are internally interconnected and, hence, almost no power losses appear in that second chip. Conversely, for $V_{\text{OC}} \geq 200$ mV (i.e., when the TEG was directly connected to ADP5092), the circuit showed an efficiency almost equal to that obtained before in Figure 6. Comparing Figures 4 and 10, one realizes that, after the selected threshold voltage of 200 mV, the circuit in Figure 8 clearly provides higher values of efficiency. On the other hand, the comparison between Figures 6 and 10 shows that the circuit in Figure 8 evidently operates from lower values of input voltage. Therefore, the proposed circuit in Figure 8 is really able to combine the benefits of both topologies.

 doi:10.20944/preprints202605.1451.v1

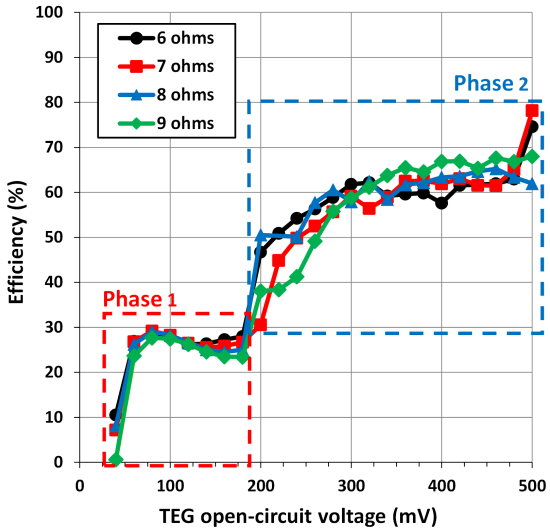

Figure 10. Experimental results of power efficiency from the circuit in Figure 8 for different values of R_{TEG}.

7. Conclusions

In the context of thermal energy harvesters for autonomous sensors, this article has proposed the interconnection of two different types of PMC to improve the overall performance in terms of both power efficiency and minimum input voltage. The proposed circuit has been experimentally characterized using commercial off-the-shelf components. Thanks to the interconnection, the resulting circuit is able to start operating from 40 mV of TEG open-circuit voltage with an overall power efficiency that can be up to 78 %.

Author Contributions: Conceptualization, M.R., F.R.; methodology, M.R., F.R.; experimental tests, F.L.; data analysis, F.L., F.R.; writing—original draft preparation, F.L., F.R.; writing—review and editing, F.L., M.R., F.R.; supervision, F.R.; funding acquisition, F.R. All authors have read and agreed to the published version of the manuscript.

Funding: This work was supported in part by MICIU/AEI/10.13039/501100011033 under Grant PID2022-139505OB-I00.

Institutional Review Board Statement: Not applicable.

Informed Consent Statement: Not applicable.

Data Availability Statement: The data that support the findings of this study are available upon reasonable request from the author.

Conflicts of Interest: The author declares no conflict of interest.

References

1. Kanoun, O.; Bouattour, G.; Khriji, S.; Hamza, K.; Adawy, A.; Bradai, S. Sustainable Wireless Sensor Networks for Railway Systems Powered by Energy Harvesting from Vibration. *IEEE Instrumentation Measurement Magazine* **2023**, *26*, 33–38. https://doi.org/10.1109/MIM.2023.10121388.
2. Mathews, I.; Kantareddy, S.N.; Buonassisi, T.; Peters, I.M. Technology and Market Perspective for Indoor Photovoltaic Cells. *Joule* **2019**, *3*, 1415–1426.
3. Pecunia, V.; Occhipinti, L.G.; Hoye, R.L.Z. Emerging Indoor Photovoltaic Technologies for Sustainable Internet of Things. *Advanced Energy Materials* **2021**, *11*, 2100698.
4. Reverter, F.; Du, S. Board-Level Power Management Circuits for Triboelectric Nanogenerators: A Review. *IEEE Transactions on Power Electronics* **2026**, *41*, 12274–12286. https://doi.org/10.1109/TPEL.2026.3659208.
5. Ferré, E.; Martinez, B.; Villaverde, M.; Gasulla, M.; Reverter, F. Low-Area PV Cells Under Indoor Artificial Lighting: A Comparative Study. *IEEE Transactions on Instrumentation and Measurement* **2025**, *74*, 1–9.

 doi:10.20944/preprints202605.1451.v1

6. Reverter, F. Study of Low-Area PV Modules Under Indoor Natural Daylight for Autonomous Sensors. *IEEE Sensors Letters* **2025**, *9*, 1–4.
7. Panbude, A.; Veluswamy, P. Self-Powered Standalone Performance of Thermoelectric Generator for Body Heat Harvesting. *IEEE Sensors Letters* **2024**, *8*, 1–4. https://doi.org/10.1109/LSENS.2024.3456289.
8. Ridwan, M.; Gasulla, M.; Reverter, F. Principle and Applications of Thermoelectric Generators: A Review. *Sensors* **2025**, *25*. https://doi.org/10.3390/s25082484.
9. Hamza, K.; Bouattour, G.; Benbrahim, F.; Bader, S.; Fakhfakh, A.; Kanoun, O. A Robust Energy Management Circuit for Energy Harvesting From Wideband Low-Acceleration Vibrations in Wireless Sensor Screws. *IEEE Sensors Letters* **2025**, *9*, 1–4. https://doi.org/10.1109/LSENS.2025.3592235.
10. Bakhtiar, S.; Masabi, S.N.; Li, T.; Papuga, J.; West, A.; Jiang, J.; Theodossiades, S. Energy Harvesting from Clustered Piezoelectric Beams for Aircraft Health Monitoring Systems. *Applied Sciences* **2026**, *16*. https://doi.org/10.3390/app16073115.
11. Saab, S.; Kouzayha, N.; Eid, A.; Benbuk, A.A.; Costantine, J.; Dawy, Z. Recycling Ambient Wi-Fi Signals for Low Energy Wake-Up of Wireless Sensors. *IEEE Sensors Letters* **2020**, *4*, 1–4. https://doi.org/10.1109/LSENS.2020.3026236.
12. Dalola, S.; Ferrari, M.; Ferrari, V.; Guizzetti, M.; Marioli, D.; Taroni, A. Characterization of Thermoelectric Modules for Powering Autonomous Sensors. *IEEE Transactions on Instrumentation and Measurement* **2009**, *58*, 99–107. https://doi.org/10.1109/TIM.2008.928405.
13. Baca, T.; Sarafin, P.; Chochul, M.; Kubascik, M. Thermoelectric Transducers: A Promising Method of Energy Generation for Smart Roads. *Applied Sciences* **2026**, *16*. https://doi.org/10.3390/app16031662.
14. Tran-Dinh, T.; Pham, H.M.; Pham-Nguyen, L.; Lee, S.G.; Le, H.P. Power Management IC With a Three-Phase Cold Self-Start for Thermoelectric Generators. *IEEE Transactions on Circuits and Systems I: Regular Papers* **2021**, *68*, 103–113. https://doi.org/10.1109/TCSI.2020.3023252.
15. Azlor, M.; Martinez, B.; Gasulla, M.; Reverter, F. Study of the Applicability and Limitations of the FOCV Technique for Indoor Low-Area PV Cells. *IEEE Transactions on Instrumentation and Measurement* **2025**, *74*, 1–9.
16. Lohrabi Pour, F.; Hong, S.K.; Lee, J.; Sohani Darban, M.; Kim, J.M.; Ha, D.S. Three-Phase Powerline Energy Harvesting Circuit with Maximum Power Point Tracking and Cold Start-Up. *Applied Sciences* **2025**, *15*. https://doi.org/10.3390/app152211954.
17. Shang, Z.; Zhao, Y.; Gou, W.; Geng, L.; Lian, Y. 83.9% Efficiency 100-mV Self-Startup Boost Converter for Thermoelectric Energy Harvester in IoT Applications. *IEEE Transactions on Circuits and Systems II: Express Briefs* **2020**, *67*, 1654–1658. https://doi.org/10.1109/TCSII.2020.2999331.
18. Ridwan, M.; Gasulla, M.; Reverter, F. Study of TEG-Heatsink Pairs for Indoor Thermal Energy Harvesting Applications. In Proceedings of the 2025 IEEE Sensors Applications Symposium (SAS), 2025, pp. 1–5. https://doi.org/10.1109/SAS65169.2025.11105192.
19. Lallart, M.; Phung, L.V.; Massot, B. Transformer-Free, Off-the-Shelf Electrical Interface for Low-Voltage DC Energy Harvesting. *IEEE Transactions on Industrial Electronics* **2018**, *65*, 5580–5589. https://doi.org/10.1109/TIE.2017.2777402.
20. Qian, Y.; Lu, D.; He, J.; Hong, Z. An On-Chip Transformer-Based Self-Startup Hybrid SIDITO Converter for Thermoelectric Energy Harvesting. *IEEE Transactions on Circuits and Systems II: Express Briefs* **2018**, *65*, 1673–1677. https://doi.org/10.1109/TCSII.2017.2773564.
21. Estrada-López, J.J.; Castillo-Atoche, A.A.; Sanchez-Sinencio, E. Design and Fabrication of a 3-D Printed Concentrating Solar Thermoelectric Generator for Energy Harvesting Based Wireless Sensor Nodes. *IEEE Sensors Letters* **2019**, *3*, 1–4. https://doi.org/10.1109/LSENS.2019.2948811.
22. Xia, C.; Zhang, D.; Pedrycz, W.; Fan, K.; Guo, Y. Human Body Heat Based Thermoelectric Harvester with Ultra-Low Input Power Management System for Wireless Sensors Powering. *Energies* **2019**, *12*.
23. Lv, J.R.; Ma, J.L.; Dai, L.; Yin, T.; He, Z.Z. A high-performance wearable thermoelectric generator with comprehensive optimization of thermal resistance and voltage boosting conversion. *Applied Energy* **2022**, *312*, 118696. https://doi.org/https://doi.org/10.1016/j.apenergy.2022.118696.
24. Reverter, F.; Gasulla, M. Optimal Inductor Current in Boost DC/DC Converters Regulating the Input Voltage Applied to Low-Power Photovoltaic Modules. *IEEE Transactions on Power Electronics* **2017**, *32*, 6188–6196. https://doi.org/10.1109/TPEL.2016.2619482.

 doi:10.20944/preprints202605.1451.v1

disclaim responsibility for any injury to people or property resulting from any ideas, methods, instructions or products referred to in the content.